Nuclear Engineering and Technology 53 (2021) 282–293

Contents lists available at ScienceDirect

Nuclear Engineering and Technology

journal homepage: www.elsevier.com/locate/net

Original Article

Investigations on borate glasses within SBC-Bx system for gamma-ray shielding applications

Y.S. Rammah [a], H.O. Tekin [b], C. Sriwunkum [c], I. Olarinoye [d], Amani Alalawi [e], M.S. Al-Buriahi [f, *], T. Nutaro [c], Baris T. Tonguc [f]

[a] Physics Department, Menoufia University, 32511, Shebin El Koom, Egypt
[b] Department of Medical Diagnostic Imaging - College of Health Sciences University of Sharjah, Sharjah, United Arab Emirates
[c] Department of Physics, Ubon Ratchathani University, Ubon Ratchathani, Thailand
[d] Department of Physics, Federal University of Technology, Minna, Nigeria
[e] Department of Physics, Umm AL-Qura University, Makkah, Saudi Arabia
[f] Department of Physics, Sakarya University, Sakarya, Turkey

ARTICLE INFO

Article history:
Received 7 September 2019
Received in revised form
25 June 2020
Accepted 30 June 2020
Available online 18 July 2020

Keywords:
Gamma shielding
Borate glass
PHITS code
XCOM

ABSTRACT

This paper examines gamma-ray shielding properties of SBC-Bx glass system with the chemical composition of $40SiO_2$–$10B_2O_3$–xBaO–(45-x)CaO– yZnO– zMgO (where $x = 0, 10, 20, 30$, and 35 mol% and $y = z = 6$ mol%). Mass attenuation coefficient (μ/ρ) which is an essential parameter to study gamma-ray shielding properties was obtained in the photon energy range of 0.015–15 MeV using PHITS Monte Carlo code for the proposed glasses. The obtained results were compared with those calculated by WinXCOM program. Both the values of PHITS code and WinXCOM program were observed in very good agreement. The μ/ρ values were then used to derive mean free path (MFP), electron density (N_{eff}), effective atomic number (Z_{eff}), and half value layer (HVL) for all the glasses involved. Additionally, G-P method was employed to estimate exposure buildup factor (EBF) for each glass in the energy range of 0.015–15 MeV up to penetration depths of 40 mfp. The results reveal that gamma-ray shielding effectiveness of the SBC-Bx glasses evolves with increasing BaO content in the glass sample. Such that SBC-B35 glass has superior shielding capacity against gamma-rays among the studied glasses. Gamma-ray shielding properties of SBC-B35 glass were compared with different conventional shielding materials, commercial glasses, and newly developed HMO glasse. Therefore, the investigated glasses have potential uses in gamma shielding applications.

© 2020 Korean Nuclear Society, Published by Elsevier Korea LLC. This is an open access article under the CC BY-NC-ND license (http://creativecommons.org/licenses/by-nc-nd/4.0/).

1. Introduction

Progress and development technologies have brought many risk for humanity. For example, people may be exposed to low or high photon energies whether this is in X-ray rooms, nuclear power plants, or laboratories. These photons can travel fast and also can penetrate deeply through materials. An excessive exposure to such photons could cause many harmful effects such as genetic disorders, cataracts, cancer and possibly death [1]. This triggered many scientists to pay tremendous efforts for studying gamma-ray interaction properties with different types of shielding materials [2–4]. In this regard, different materials such as alloys, ceramics, concrete, rocks and polymers are utilized as shielding materials against gamma-ray radiation [5–13]. Although these materials are low cost and widely available, they also have many disadvantages such as they are not transparent to the visible light, cracks formation and water permeability [14–16]. On the contrary, glass materials are transparent to the light and can be used to design doors and windows in medical and nuclear establishments. Also, glasses have many unique mechanical and physical advantages such as hardness, excellent corrosion resistance, and ease of preparation by different methods [17–20].

Recently, many experimental, theoretical, and Monte Carlo Simulation (MCS) studies were carried out to study the gamma-ray shielding properties of different glass compositions [4,5,7,9,12–14,17,21–27]. The significant finding of these studies is that the heavy metal oxides (HMO) play an important role to evolve

---

* Corresponding author.,

E-mail addresses: mburiahi@gstd.sci.cu.edu.eg, mohammed.al-buriahi@ogr.sakarya.edu.tr (M.S. Al-Buriahi).

https://doi.org/10.1016/j.net.2020.06.034

1738-5733/© 2020 Korean Nuclear Society, Published by Elsevier Korea LLC. This is an open access article under the CC BY-NC-ND license (http://creativecommons.org/licenses/by-nc-nd/4.0/).

the gamma-ray shielding properties. For example, the glass system of B_2O_3-ZnO-MgO-Bi_2O_3 offers the best performance to block gamma-ray radiation as Bi_2O_3 content increases in the glass sample [23]. Further, Vani et al. concluded that the glasses doping with heavy elements like barium led to improve the efficient shielding materials [24]. Tekin et al. proposed many samples among SPCG glasses which showed clear advantages to use as shielding against the X- and gamma rays [25]. Agar et al. studied BaO, MoO_3 and P_2O_5 based glasses using MCS [26]. Among the studied glasses, it was found that BaMoP8 glass sample has an excellent gamma-ray shielding features. Finally, Sayyed et al. evaluated the gamma-ray shielding features for new glass system. This study was found that Bi40B20 glass which contains the highest B_2O_3 mol % becomes the best glass to attenuate gamma-ray [27].

The radiation shielding properties of any composed material such as glass can be tested by determinig several parameters such as μ/ρ, HVL, Z_{eff}, MFP, and EBF. The μ/ρ is considered as a key parameter to characterize gamma photons interaction with shields as well as to calculate the other aforementioned shielding parameters. One way to obtain μ/ρ is experimentally by using the well-known transmission geometry. However, this method is restricted to limited photon energies as well as other difficulties in the samples preparation and radiation safety [28,29]. Therefore, it has mushroomed among researchers that MCS is the best way to study the gamma-ray shielding properties of materials [29–31]. Geant4 code was employed for several similar studies as well as MCNPX, PHITS, and FLUKA codes were also carried out to achieve many successful works [30,32–34]. Moreover, exposure buildup factor (EBF) is a significant parameter in predicting and evaluating the distribution of gamma flux in a material [35]. EBF values were obtained by different methods such as invariant embedding method which applied for 26 materials up to depths of 100 mfp [36]. However, Geometric Progression (G-P) formula is the most suitable method to calculate EBF [3,37,38]. This method is widely applied for photon energy in the range of 0.015–15 MeV. Very recently, the SBC-Bx glass system was studied in terms of gamma shielding properties by using PHITS and FLUKA codes for a short energy range between 356 keV and 2.51 MeV [39]. This study showed promising properties of the SBC-Bx glass system, and this encouraged us to establish an extentened investigation of the SBC-Bx glass system.

In the present work, SBC-Bx glass system with the chemical composition of $40SiO_2$–$10B_2O_3$–xBaO–(45-x)CaO–yZnO–zMgO (where x = 0, 10, 20, 30, and 35 mol% and y = z = 6 mol%) have been studied to serve in various radiation shielding applications. PHITS code and Geant4 toolkit were carried out to simulate the narrow beam experiment to investigate gamma-ray shielding paramters such as μ/ρ, Z_{eff}, HVL, and MFP. The results obtained by PHITS Monte Carlo code were compared with those of WinXCOM program. The EBF values for each glass were also calculated in the energy range of 0.015–15 MeV up to penetration depths of 40 mfp. The radiation shielding properties of the proposed glasses were compared with some competing shielding materials. This study would be useful for scientific community to move up the progress in radiation protection field.

2. Gamma shielding properties

2.1. Mass attenuation coefficient (μ/ρ)

Gamma photon experiences an attenuation as it passes a certain material thickness. More attenuation for a given thickness refers more preferable shielding material. Therefore, the selection of shielding material depends mainly on attenuation degree which is expressed by Lambert-Beer law [40]:

$$I = I_0 e^{-\mu x} \tag{1}$$

where I is an attenuated photon intensity, I_0 is an incident photon intensity, μ (cm^{-1}) is the linear attenuation coefficient and x is the thickness of the material. This law is valid for all materials when the gamma photon is monochromatic. In order to study the shielding capacity of the material, it is reasonable to deal with mass attenuation coefficient (μ/ρ) in a unit of cm^2g^{-1}. For composite materials (e.g. glass), the μ/ρ is given at certain photon energy by the following relation [34,41]:

$$\mu\Big/\rho = \sum_i w_i(\mu/\rho)_i \tag{2}$$

where w_i is a weight fraction of ith constituent element in the shielding material sample and $(\mu/\rho)_i$ is a total mass attenuation coefficient of that element at certaion photon energy.

2.2. Effective atomic number (z_{eff})

The Z_{eff} refers to the attenuation of the gamma-rays that occurs due to the partial photon interactions with matter and it is given by the following equation [41,42]:

$$Z_{eff} = \frac{\sum_i f_i A_i \left(\frac{\mu}{\rho}\right)_i}{\sum_j f_j (A_j/Z_j) \left(\frac{\mu}{\rho}\right)_j} \tag{3}$$

Where μ/ρ is the mass attenuation coefficient. f_i is the fractional abundance of the element inside the glass sample, and A_i is the atomic weight. The effective electron density (N_{eff}) is given by the relation of [43];

$$N_{eff} = N_A \frac{n Z_{eff}}{\sum_i n_i A_i} \quad (electrons\,/\,g) \tag{4}$$

2.3. Half-value layer (HVL)

Half-value layer is a very useful parameter to study the shielding properties of gamma-ray and to estimate the penetrating power of gamma radiation inside the sample. HVL is the thickness that attenuates the incident photon intensity by one half and it indicates to the penetration ability of the photons as the energy increases. HVL values have been calculated for the present glasses by applying the next formula [44,45]:

$$HVL = \frac{\ln(2)}{\mu} \tag{5}$$

2.4. Mean free path (MFP)

The mean free path is the average distance between two successive collisions by the photons and can be obtained according to the equation [46,47]:

$$MFP = \frac{1}{\mu} \tag{6}$$

2.5. Exposure buildup factor (EBF)

EBF is a correction term resulting from secondary particles that are mostly related to Compton scattering. EBF can be computed by using the interpolation method for the equivalent atomic number (Z_{eq}) according to the following equation [43].

$$Z_{eq} = \frac{Z_1(\log R_2 - \log R) + Z_2(\log R - \log R_1)}{\log R_2 - \log R_1} \tag{7}$$

where R is the ratio of $(\mu_m)_{Comp}$ and $(\mu_m)_{total}$ for a given glass, Z_1 and Z_2 are related to the ratio R_1 and R_2 respectively. The calculated Z_{eq} values for the glasses were then used to calculate the five parameters (b, c, a, X_K and d) of G-P fitting by using the formula [32].

$$P = \frac{P_1(\log Z_2 - \log Z_{eq}) + P_2(\log Z_{eq} - \log Z_1)}{\log Z_2 - \log Z_1} \tag{8}$$

where P_1 and P_2 are the G-P fitting parameters, respectively. More details were reported by Refs. [48]. Finally, EBF values can be obtained by the following equations [32,43].

$$B(E,X) = 1 + \frac{b-1}{K-1}(K^x - 1) \quad for \quad K \neq 1 \tag{9}$$

$$B(E,X) = 1 + (b-1)x \quad for \quad K = 1 \tag{10}$$

where,

$$K(E,X) = cx^a + d\frac{\tanh\left(\frac{x}{X_k} - 2\right) - \tanh(-2)}{1 - \tanh(-2)} \quad for \quad x \leq 40 \tag{11}$$

where x refers to mfp, E refers to the incident energy, and K(E,X) refers to the absorbed dose [3,48].

3. PHITS Monte Carlo code

PHITS is a general-purpose Carlo particle transport simulation code developed by JAEA [49]. This code can deal with several nuclear reaction models and nuclear data libraries for simulating many types of particles collision process and interactions with matter over wide energy range. The simulation parameters such as materials composition, spatial geometry configuration, source specification, and external environment have to define in a PHITS data card with [Parameters], [Material], [Surface], [Cell] and [Source] categories.

In this work, we have performed the narrow beam transmission geometry which consists of radiation source, glass sample target, detector cell, lead containers and collimators as shown in Fig. 1. This

Fig. 1. A total-3D view of designed simulation geometry by using PHITS code.

geometry is virtually the same as the experimental transmission geometry used in Refs. [50–52].A disk gamma source of diameter 0.5 cm, having different photon energies ranging from 0.015 to 15 MeV, was enclosed in the lead container and placed front left the glass sample. A disc of glass sample with various thicknesses (d) was defined as the absorber material and placed 66 cm at distance from the front face of the detection area. The detection cell considered in the simulation is sodium iodide (NaI) crystal, with 7.62 cm in diameter and 7.62 cm in height adapted from Refs. [53]. The glass sample specifications including calculated weight fractions of each constituent and densities of the present SiO2-B2O3-BaO-CaO-ZnO-MgO glass systems were designated in the PHITS material card, as given in Table 1. When photon interacted with glass sample passing through a detection cell, incident (f_0) and transmitted (f) photon fluences were evaluated by utilizing tally and estimator cards. In PHITS simulations, T-Track tally card was used to score average particle fluence determined by dividing tallied track lengths by the detection cell volume and the number of source particles. Then, μ/ρ for the investigated glass were calculated by applying the well-known Beer-Lambert law Eq. (1). In simulation code, statistical uncertainties of the results were less than 0.1 %, achieved for the number of photon histories being 10 million. The obtained results from PHITS code were compared with theoretical values calculated by XCOM program [54].

4. Results and discussion

4.1. Mass attenuation coefficients

Table 1 shows the sample code, density, and fractional weight for $SiO_2-B_2O_3-BaO-CaO-ZnO-MgO$ glass system. From Table 1, one can see that the density values for these glasses increase from 2.89 to 3.46 (g/cm^3) as BaO content increases from 0 to 35 mol %. The reason can be explained by that the atomic weight of BaO (153.326 g/mol) is higher than that of CaO (56.077 g/mol). Therefore, the glass matrix becomes denser by adding more amount of BaO content into the glass network.

The μ/ρ values for these glasses were determined using PHITS simulation code in the photon energy ranges between 0.015 and 15 MeV. The validation of the simulation values with theoretical predictions plays a basic role to know the accuracy of the present results. Thus, PHITS results of μ/ρ were compared to the theoretical values obtained using XCOM software. Table 2 and 3 show the results of PHITS, XCOM, and the deviation between theoretical results (XCOM) and simulation values (PHITS) of μ/ρ for all of the studied glasses. It is clear that the theoretical and simulation results of μ/ρ are in good agreement. The deviation between PHITS simulations and XCOM values was evaluated according to the following equation [55]:

$$Dev. = \left|\frac{(\mu/\rho)_{XCOM} - (\mu/\rho)_{PHITS}}{(\mu/\rho)_{XCOM}} \times 100\right| \tag{12}$$

We found that the difference between the theoretical values (XCOM) and simulated values (PHITS) is less than 2 % and this confirms the accuracy of the present results (see Table 3). Moreover, Table 4 and Table 5 show the results of Geant4 simulations and XCOM standard database. The comparison between PHITS simulation (Table 2 and 3) and Geant4 simulation (Table 4 and 5), shows that PHITS simulation is superior than Geant4 simulation in terms of the lower deviation with the XCOM standard database. Fig. 2 shows the variation of μ/ρ with both the photon energy and the chemical composition for each glass sample. It is obvious that the μ/ρ decreases with increasing the photon energy, and it increases with increasing BaO content in the glass sample. The μ/ρ values of
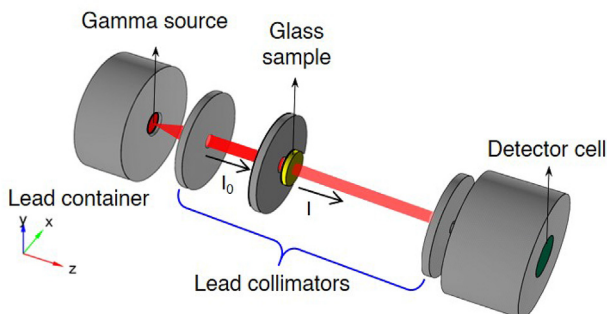
Table 1
Sample code, density, and atomic composition of barium borate glass system with the chemical composition of $40SiO_2-10B_2O_3-xBaO-(45-x)CaO-yZnO-zMgO$ (where x = 0, 10, 20, 30, and 35 mol% and y = z = 6 mol%).

Sample Code	Density (g/cm^3)	Atomic composition (wt.%)						
		B	O	Mg	Si	Ca	Zn	Ba
SBC-B00	2.89	0.02773	0.41093	0.03231	0.16694	0.31906	0.04304	0.00000
SBC-B10	3.06	0.02773	0.39477	0.03231	0.16694	0.25525	0.04304	0.07997
SBC-B20	3.23	0.02773	0.37861	0.03231	0.16694	0.19144	0.04304	0.15994
SBC-B30	3.37	0.02773	0.36245	0.03231	0.16694	0.12762	0.04304	0.23991
SBC-B35	3.46	0.02773	0.35438	0.03231	0.16694	0.09572	0.04304	0.27989

the glasses are found to be large around 15 keV and gradually decrease as photon energy increases. This can be explained on the base of the photon partial interaction processes. In the low energy region (e.g around 356 keV), the attenuation is governed by the law of photoelectric absorption which is proportional inversely to E^3. In the high energy region (e.g 0.2–4 MeV) Compton scattering dominates the attenuation process and this is proportional inversely to E. Beyond 4 MeV the μ/ρ values seem to be constant due to the pair production process dominates in this region. On the other hand, the attenuation ability of the glass is strongly related to the chemical composition of the glass. Such that gamma photons experience higher attenuation as the BaO content increases in the glass sample. Moreover, It is seen clearly that the curve of SBC-B00 glass (without BaO content) is typical without any peak, while there are peaks in the other curves. These peaks occur at 37.44 keV (K-absorption edge of Ba) due to the photoelectric effect. Further, by increasing the BaO content in the samples the peaks become more clear and high. As a result of aforementioned discussion we can conclude that the SBC-

B35 glass has a superior ability to attenuate gamma-ray among our proposed glasses. Consequently, it is worthy to compare the attenuation ability of SBC-B35 glass with other conventional materials and commercial glasses (see Fig. 3). From Fig. 3, it is seen that the mass attenuation cofficient values of SBC-B35 are higher than those of RS-253-G18 glass, window glass type A, and ordinary concrete taken from Ref. [56,57], and [58], respectively.

4.2. Effective atomic number (z_{eff})

In order to investigate the shielding effectiveness of the glasses to serve in gamma shielding applications, we also calculated Z_{eff}. Fig. 4 shows the calculated values of Z_{eff} for all the glasses and their variation with both the photon energy and the chemical composition of the glass. The Z_{eff} values of the present glasses vary from 11.21 to 18.78 for SBC-B00 glass, from 12.69 to 22.54 for SBC-B10 glass, from 14.09 to 26.33 for SBC-B20 glass, from 15.55 to 29.77 for SBC-B30 glass, and from 16.24 to 31.40 for SBC-B35 glass. It is

Table 2
Comparison of theoretical mass attenuation coefficient (μ/ρ) values with those obtained by PHITS simulation code for $SiO_2-B_2O_3-BaO-CaO-ZnO-MgO$ glass system.

E (keV)	SBC-B00			SBC-B10			SBC-B20		
	XCOM	PHITS	%Dev.[a]	XCOM	PHITS	%Dev.[a]	XCOM	PHITS	%Dev.[a]
0.015	15.6979	15.4727	1.43	18.8420	18.9364	0.50	21.9860	21.7134	1.24
0.02	6.9659	7.0706	1.50	8.4678	8.5170	0.58	9.9696	10.0379	0.68
0.03	2.2517	2.2692	0.78	2.7772	2.7785	0.05	3.3028	3.3028	0.00
0.04	1.0598	1.0645	0.45	2.9037	2.8996	0.14	4.7477	4.7408	0.14
0.05	0.6259	0.6308	0.80	1.6600	1.6637	0.22	2.6941	2.6953	0.05
0.06	0.4303	0.4309	0.15	1.0658	1.0679	0.20	1.7013	1.7051	0.22
0.08	0.2692	0.2694	0.08	0.5601	0.5602	0.02	0.8510	0.8516	0.08
0.1	0.2071	0.2076	0.23	0.3638	0.3636	0.04	0.5204	0.5210	0.11
0.15	0.1515	0.1517	0.14	0.2012	0.2010	0.13	0.2509	0.2507	0.08
0.2	0.1301	0.1307	0.43	0.1517	0.1522	0.29	0.1733	0.1737	0.21
0.3	0.1087	0.1090	0.26	0.1150	0.1151	0.13	0.1212	0.1212	0.02
0.4	0.0962	0.0967	0.57	0.0985	0.0989	0.42	0.1009	0.1012	0.30
0.5	0.0874	0.0878	0.47	0.0883	0.0886	0.35	0.0891	0.0893	0.23
0.6	0.0806	0.0809	0.42	0.0808	0.0811	0.31	0.0810	0.0812	0.23
0.8	0.0706	0.0707	0.15	0.0703	0.0704	0.06	0.0700	0.0700	0.01
1	0.0634	0.0635	0.09	0.0629	0.0629	0.03	0.0625	0.0624	0.12
2	0.0446	0.0445	0.30	0.0443	0.0441	0.40	0.0439	0.0436	0.83
3	0.0366	0.0361	1.44	0.0366	0.0361	1.39	0.0365	0.0359	1.82
4	0.0322	0.0318	1.32	0.0324	0.0320	1.28	0.0326	0.0321	1.68
5	0.0295	0.0290	1.68	0.0299	0.0294	1.62	0.0303	0.0298	1.65
6	0.0277	0.0272	1.60	0.0283	0.0278	1.57	0.0288	0.0284	1.62
7	0.0264	0.0259	1.91	0.0271	0.0267	1.79	0.0279	0.0274	1.88
8	0.0255	0.0251	1.48	0.0264	0.0260	1.35	0.0272	0.0269	1.32
9	0.0248	0.0244	1.92	0.0258	0.0254	1.61	0.0268	0.0264	1.54
10	0.0244	0.0241	1.17	0.0254	0.0252	0.99	0.0265	0.0263	0.90
15	0.0232	0.0231	0.34	0.0247	0.0246	0.25	0.0262	0.0261	0.29

[a] Deviation between theory (XCOM) and simulation (PHITS).

Table 3
Comparison of theoretical mass attenuation coefficient (μ/ρ) values with those obtained by PHITS simulation code for SiO$_2$–B$_2$O$_3$–BaO–CaO–ZnO–MgO glass system.

E (keV)	SBC-B30			SBC-B35		
	XCOM	PHITS	%Dev.[a]	XCOM	PHITS	%Dev.[a]
0.015	25.1300	24.9313	0.79	26.7020	26.6600	0.16
0.02	11.4715	11.4940	0.20	12.2224	12.1793	0.35
0.03	3.8283	3.8223	0.16	4.0911	4.0841	0.17
0.04	6.5916	6.5784	0.20	7.5136	7.4876	0.35
0.05	3.7282	3.7281	0.00	4.2453	4.2463	0.03
0.06	2.3369	2.3364	0.02	2.6546	2.6574	0.10
0.08	1.1418	1.1435	0.14	1.2873	1.2885	0.09
0.1	0.6771	0.6773	0.04	0.7554	0.7551	0.04
0.15	0.3007	0.3004	0.09	0.3255	0.3251	0.11
0.2	0.1949	0.1951	0.13	0.2057	0.2058	0.09
0.3	0.1275	0.1276	0.05	0.1307	0.1306	0.01
0.4	0.1032	0.1034	0.20	0.1044	0.1045	0.12
0.5	0.0900	0.0901	0.14	0.0905	0.0906	0.12
0.6	0.0813	0.0814	0.15	0.0814	0.0815	0.10
0.8	0.0697	0.0697	0.06	0.0696	0.0695	0.12
1	0.0620	0.0619	0.20	0.0618	0.0616	0.25
2	0.0436	0.0433	0.61	0.0434	0.0431	0.66
3	0.0365	0.0359	1.51	0.0365	0.0359	1.48
4	0.0329	0.0324	1.33	0.0330	0.0325	1.32
5	0.0307	0.0303	1.56	0.0309	0.0305	1.54
6	0.0294	0.0290	1.36	0.0297	0.0293	1.42
7	0.0286	0.0282	1.57	0.0290	0.0285	1.53
8	0.0281	0.0278	1.19	0.0285	0.0282	1.20
9	0.0278	0.0274	1.42	0.0283	0.0279	1.41
10	0.0276	0.0274	0.83	0.0281	0.0279	0.88
15	0.0277	0.0276	0.24	0.0285	0.0284	0.28

[a] Deviation between theory (XCOM) and simulation (PHITS).

Table 5
Comparison of theoretical mass attenuation coefficient (μ/ρ) values with those obtained by Geant4 simulation code for SiO$_2$–B$_2$O$_3$–BaO–CaO–ZnO–MgO glass system.

E (keV)	SBC-B30			SBC-B35		
	XCOM	Geant4	%Dev.[b]	XCOM	Geant4	%Dev.[b]
1.50E-02	25.130	24.684	1.77	26.702	26.298	1.51
2.00E-02	11.472	11.267	1.78	12.222	12.030	1.58
3.00E-02	3.828	3.789	1.02	4.091	4.015	1.85
4.00E-02	6.592	6.520	1.08	7.514	7.377	1.81
5.00E-02	3.728	3.694	0.91	4.245	4.200	1.07
6.00E-02	2.337	2.308	1.24	2.655	2.639	0.57
8.00E-02	1.142	1.126	1.39	1.287	1.273	1.15
1.00E-01	0.677	0.671	0.90	0.755	0.749	0.84
1.50E-01	0.301	0.297	1.30	0.326	0.322	0.94
2.00E-01	0.195	0.193	1.01	0.206	0.204	0.95
3.00E-01	0.128	0.126	1.18	0.131	0.129	0.94
4.00E-01	0.103	0.102	1.18	0.104	0.103	1.11
5.00E-01	0.090	0.089	1.09	0.091	0.090	0.91
6.00E-01	0.081	0.081	0.65	0.081	0.080	1.37
8.00E-01	0.070	0.069	1.37	0.070	0.069	1.31
1.00E+00	0.062	0.062	0.54	0.062	0.061	0.97
1.50E+00	0.044	0.043	1.38	0.043	0.043	1.30
2.00E+00	0.037	0.036	0.76	0.037	0.036	1.50
3.00E+00	0.033	0.033	0.84	0.033	0.033	0.52
4.00E+00	0.031	0.030	1.10	0.031	0.031	1.26
5.00E+00	0.029	0.029	0.69	0.030	0.029	1.03
6.00E+00	0.029	0.028	1.13	0.029	0.029	0.99
8.00E+00	0.028	0.028	1.35	0.029	0.028	1.19
1.00E+01	0.028	0.027	1.48	0.028	0.028	1.35
1.50E+01	0.028	0.027	0.95	0.028	0.028	1.34

[b] Deviation between theory (XCOM) and simulation (Geant4).

Table 4
Comparison of theoretical mass attenuation coefficient (μ/ρ) values with those obtained by Geant4 simulation code for SiO$_2$–B$_2$O$_3$–BaO–CaO–ZnO–MgO glass system.

E (keV)	SBC-B00			SBC-B10			SBC-B20		
	XCOM	Geant4	%Dev.[b]	XCOM	Geant4	%Dev.[b]	XCOM	Geant4	%Dev.[b]
0.015	15.6979	15.4727	1.43	18.8420	18.9364	0.50	21.9860	21.7134	1.24
0.02	6.9659	7.0706	1.50	8.4678	8.5170	0.58	9.9696	10.0379	0.68
0.03	2.2517	2.2692	0.78	2.7772	2.7785	0.05	3.3028	3.3028	0.00
0.04	1.0598	1.0645	0.45	2.9037	2.8996	0.14	4.7477	4.7408	0.14
0.05	0.6259	0.6308	0.80	1.6600	1.6637	0.22	2.6941	2.6953	0.05
0.06	0.4303	0.4309	0.15	1.0658	1.0679	0.20	1.7013	1.7051	0.22
0.08	0.2692	0.2694	0.08	0.5601	0.5602	0.02	0.8510	0.8516	0.08
0.1	0.2071	0.2076	0.23	0.3638	0.3636	0.04	0.5204	0.5210	0.11
0.15	0.1515	0.1517	0.14	0.2012	0.2010	0.13	0.2509	0.2507	0.08
0.2	0.1301	0.1307	0.43	0.1517	0.1522	0.29	0.1733	0.1737	0.21
0.3	0.1087	0.1090	0.26	0.1150	0.1151	0.13	0.1212	0.1212	0.02
0.4	0.0962	0.0967	0.57	0.0985	0.0989	0.42	0.1009	0.1012	0.30
0.5	0.0874	0.0878	0.47	0.0883	0.0886	0.35	0.0891	0.0893	0.23
0.6	0.0806	0.0809	0.42	0.0808	0.0811	0.31	0.0810	0.0812	0.23
0.8	0.0706	0.0707	0.15	0.0703	0.0704	0.06	0.0700	0.0700	0.01
1	0.0634	0.0635	0.09	0.0629	0.0629	0.03	0.0625	0.0624	0.12
2	0.0446	0.0445	0.30	0.0443	0.0441	0.40	0.0439	0.0436	0.83
3	0.0366	0.0361	1.44	0.0366	0.0361	1.39	0.0365	0.0359	1.82
4	0.0322	0.0318	1.32	0.0324	0.0320	1.28	0.0326	0.0321	1.68
5	0.0295	0.0290	1.68	0.0299	0.0294	1.62	0.0303	0.0298	1.65
6	0.0277	0.0272	1.60	0.0283	0.0278	1.57	0.0288	0.0284	1.62
7	0.0264	0.0259	1.91	0.0271	0.0267	1.79	0.0279	0.0274	1.88
8	0.0255	0.0251	1.48	0.0264	0.0260	1.35	0.0272	0.0269	1.32
9	0.0248	0.0244	1.92	0.0258	0.0254	1.61	0.0268	0.0264	1.54
10	0.0244	0.0241	1.17	0.0254	0.0252	0.99	0.0265	0.0263	0.90
15	0.0232	0.0231	0.34	0.0247	0.0246	0.25	0.0262	0.0261	0.29

[b] Deviation between theory (XCOM) and simulation (Geant4).

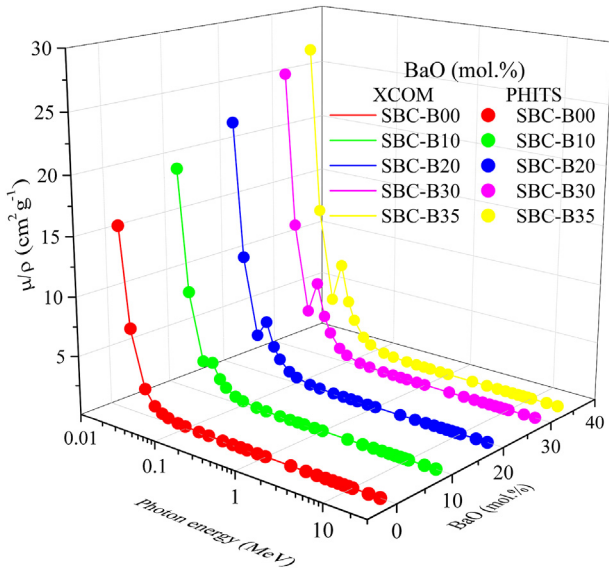**Fig. 2.** Variation of mass attenuation coefficient (cm^2/g) with photon energy for $SiO_2-B_2O_3-BaO-CaO-ZnO-MgO$ glass system by using PHITS and XCOM codes.
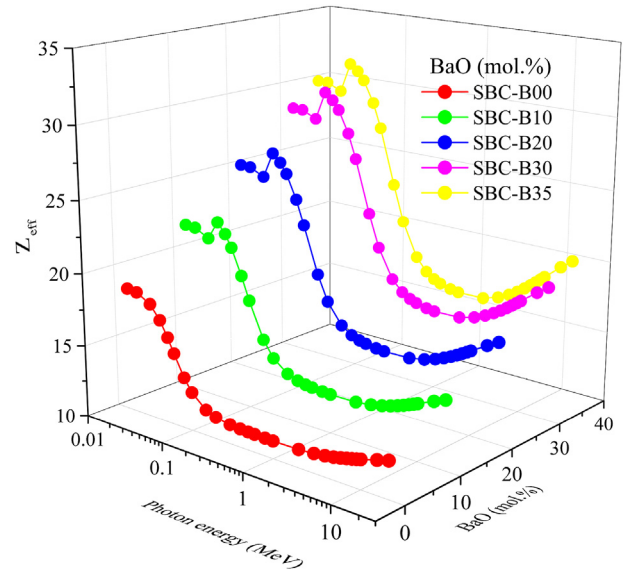

Fig. 4. Effective atomic number (Z_{eff}) as a function of photon energy for $SiO_2-B_2O_3-BaO-CaO-ZnO-MgO$ glass system.
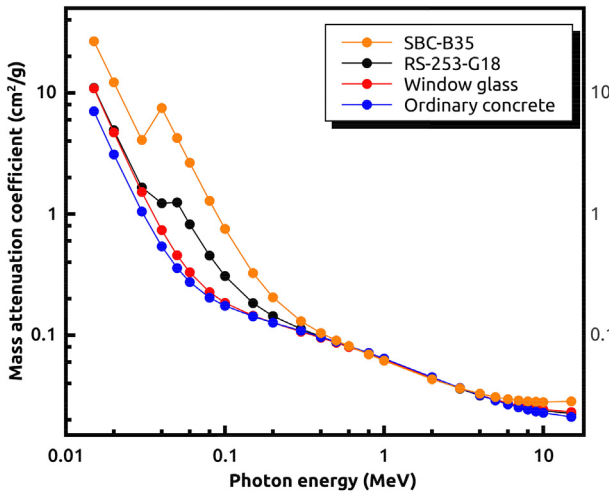

Fig. 3. Comparison of the attenuation ability of SBC-B35 glass with commercial glasses and conventional concrete.
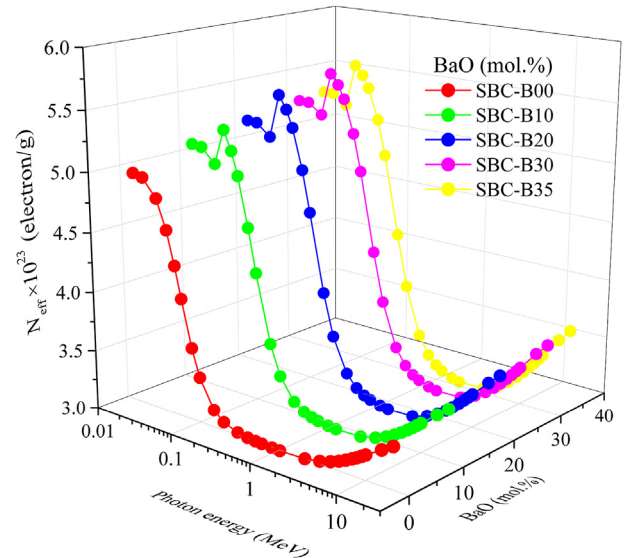

Fig. 5. Effective electron density (N_{eff}) as a function of photon energy for $SiO_2-B_2O_3-BaO-CaO-ZnO-MgO$ glass system.

found that for a given glass the maximum Z_{eff} value is observed at 0.04 MeV. It is also observed that SBC-B35 glass possesses a maximum Z_{eff}, while SBC-B00 glass possesses a minimum Z_{eff}. This is due to that the partial photon processes are directly related to Z (atomic number) of the material constituent elements. Such that the photoelectric process depends on Z^4 and the Compton process depends on Z. Therefore, Max. Z_{eff} is for SBC-B35 glass which contains the highest weight fraction of Ba (0.27989%), while the Min. Z_{eff} is for SBC-B00 glass which does not contain Ba in the glass chemical composition. In fact, the good shielding materials should

have a higher Z_{eff}. For example, the gamma-rays interact more with high Z_{eff} materials leading to decrease the photon energy that becomes incapable to penetrate the material. Thus, SBC-B35 is a better shielding material among the present glasses. By using Eq. (4), the N_{eff} can be calculated and these values are drawn in Fig. 5. From this figure, it can be seen that the behavior of N_{eff} with the photon energy is similar to that Z_{eff} for all the studied glasses. Unlike Z_{eff}, however, the N_{eff} values do not show a strong dependence of photon energy. Such that the N_{eff} values vary from 2.99 to
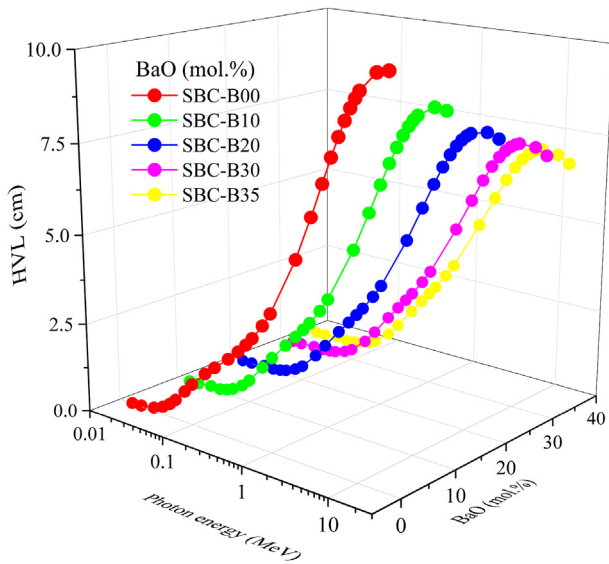
Fig. 6. Variation of half value layer (HVL) as a function of photon energy for SiO$_2$–B$_2$O$_3$–BaO–CaO–ZnO–MgO glass system.

Fig. 7. Variation of mean free path (MFP) as a function of photon energy for SiO$_2$–B$_2$O$_3$–BaO–CaO–ZnO–MgO glass system.

5.01 for SBC-B00 glass, from 2.95 to 5.25 for SBC-B10 glass, from 2.93 to 5.43 for SBC-B20 glass, from 2.88 to 5.51 for SBC-B30 glass, and from 2.86 to 5.54 for SBC-B35 glass.

4.3. Half value layer (HVL)

HVL was calculated to estimate the required thickness to attenuate half of incident gamma photons. HVL values give particular information of the shielding capacity for the studied glasses against gamma-rays (e.g. the lower HVL, the higher shielding capacity). HVL values were calculated by Eq. (5) and drawn in Fig. 6. The last figure depicts the relations between HVL − photon energy and HVL − BaO content. The HVL values increase

with increasing the photon energy, such behavior of HVL with the photon energy reflects the partial photon interactions with the glass samples. On the other hand, at a given photon energy the BaO content plays an important role to decrease the HVL values of the studied glasses. Therefore, SBC-B35 glass is a promising candidate for gamma-ray protection applications among our glasses.

4.4. Mean free path (MFP)

The average distance traveled by photon between two successive interactions is measured by MFP. The MFP values can confirm the competence of the glasses under the study to serve in gamma-ray shielding applications. Fig. 7 represents the relation between MFP - photon energy and MFP - BaO content for the studied glasses. It is clear that the MFP is small when the photon energy is low and becomes higher as the photon energy increases. Thus, in practical application it is better to increment the thickness of the glass because of the high energy photons can penetrate the glass more deeply. Moreover, it can be noted that the surplus of BaO content in the glass sample has a considerable effect to improve the shielding effectiveness of these glasses. Such that the photon interaction depends on the atomic cross sections that related to Z^4 at the low photon energies (photoelectric absorption) and related to Z at the high photon energies (Compton scattering). Thus, the probability of the photon interaction increases as Z_{eff} increases, which means that the attenuation of photons will be very high leading to decrese MFP of the glasses involved [59]. Therefore, SBC-B00 glass (with free BaO) possesses a maximum MFP, while SBC-B35 (with 35 % BaO content) possesses a minimum MFP and offers superior gamma-ray shielding properties among our proposed glasses. In Table 6 the gamma-ray shielding effectiveness of SBC-B35 glass is compared in terms of MFP with that of recently published glasses. This comparison reveals that the SBC-B35 glass has a very close equivalent shielding properties with those glasses newly developed such as Bi10 [23], TeZnBa5 [24], 0D [25], BaMoP8 [26], Pb30 [32], and Bi20B40 [27].

4.5. Exposure buildup factor (EBF)

The significant gamma-ray shielding parameters such as the equivalent atomic number (Z_{eq}) and G-P exposure buildup factor (EBF) coefficients were studied and listed in Table 7 for SBC-B35 glass system. The variation of EBF with photon energy is shown in Fig. 8 for all the glasses at different penetration depths 1, 5, 10, 20, 30, and 40 mfp. These plots are generally similar to those obtained for different glasses and concretes elsewhere [3,32]. From Fig. 8, it can be seen that the values of EBF are very small at the low photon energies due to the photoelectric effect. At the intermediate photon energies, the EBF values suddenly increased and reached the maximum in these energies. This behavior can be explained by multiple scattering events of Compton effect. Finally, due to the pair production effect in high photon energies, the EBF values slowly increased at the high penetration depths (40 mfp). Furthermore, Fig. 8 shows a strong relation between the EBF and the penetration depths for each glass sample at specific photon energy. Such this relation is that EBF increase as penetration depth, and the maximum EBF value is observed at 40 mfp for all the glasses. The reason is that secondary photons are more produced as mfp increases due to the multiple Compton interactions. Also, one can observe atypical changes (like peaks) due to absorption edges of high-Z elements such as Ba element [3]. In Fig. 9 all the studied

Table 6
Comparison of the gamma-ray shielding effectiveness of SBC-B35 glass with some competing gamma-ray shielding glasses in terms of MFP.

Energy (MeV)	SBC-B35	Bi-10 [23]	TeZn-Ba5 [24]	0D [25]	BaMo-P8 [26]	Pb-30 [32]	Bi20-B40 [27]
0.015	0.0075	0.0051	0.0041	0.0024	0.0108	0.0044	0.0029
0.02	0.0164	0.0069	0.0090	0.0033	0.0060	0.0065	0.0040
0.03	0.0489	0.0198	0.0269	0.0068	0.0171	0.0187	0.0113
0.04	0.0266	0.0415	0.0131	0.0144	0.0264	0.0398	0.0170
0.05	0.0471	0.0734	0.0235	0.0258	0.0478	0.0709	0.0302
0.06	0.0754	0.1160	0.0382	0.0415	0.0777	0.1125	0.0484
0.08	0.1554	0.2322	0.0817	0.0865	0.1650	0.2254	0.1004
0.1	0.2648	0.1111	0.1454	0.0497	0.2880	0.1143	0.0602
0.15	0.6145	0.2902	0.3821	0.1345	0.7034	0.2954	0.1628
0.2	0.9727	0.5443	0.6799	0.2629	1.1555	0.5465	0.3179
0.3	1.5310	1.1494	1.2501	0.6008	1.8944	1.1175	0.7265
0.4	1.9168	1.7310	1.6917	0.9635	2.4122	1.6425	1.1662
0.5	2.2114	2.2328	2.0319	1.2989	2.8063	2.0831	1.5739
0.6	2.4579	2.6604	2.3101	1.5960	3.1332	2.4550	1.9363
0.8	2.8751	3.3632	2.7662	2.0947	3.6808	3.0617	2.5447
1	3.2379	3.9423	3.1515	2.5076	4.1543	3.5635	3.0487
2	4.6069	5.8205	4.4658	3.7277	5.8791	5.2078	4.5495
3	5.4833	6.8136	5.1263	4.2020	6.8740	6.0721	5.1571
4	6.0695	7.3984	5.4603	4.3877	7.4680	6.5644	5.4166
5	6.4649	7.7416	5.6149	4.4368	7.8150	6.8397	5.5030
6	6.7299	7.9326	5.6701	4.4156	8.0098	6.9820	5.4985
7	6.9031	8.0231	5.6649	4.3602	8.1030	7.0401	5.4470
8	7.0129	8.0529	5.6252	4.2862	8.1319	7.0466	5.3694
9	7.0761	8.0379	5.5641	4.2052	8.1161	7.0163	5.2802
10	7.1072	7.9984	5.4928	4.1210	8.0743	6.9671	5.1860
15	7.0303	7.6371	5.1192	3.7445	7.7354	6.6139	4.7381

Table 7
Equivalent atomic number (Z_{eq}) and G-P exposure buildup factor (EBF) coefficients for SBC-B35 glass system.

Energy	Z_{eq}	b	c	a	X_k	d
0.015	19.40	1.004	1.440	−0.482	5.780	0.324
0.02	19.72	1.010	0.115	0.700	11.050	−0.864
0.03	20.18	1.022	0.362	0.202	15.530	−0.105
0.04	33.30	3.695	0.344	0.060	29.480	−0.092
0.05	34.10	2.950	0.043	−0.218	16.470	0.045
0.06	34.60	1.237	0.519	0.105	13.180	−0.051
0.08	35.26	1.212	0.273	0.387	13.590	−0.179
0.1	35.61	1.464	0.224	0.177	14.320	−0.112
0.15	35.94	1.300	0.305	0.409	14.220	−0.113
0.2	36.03	1.138	0.539	0.140	13.980	−0.069
0.3	36.17	1.247	0.501	0.174	14.390	−0.096
0.4	36.34	1.347	0.647	0.112	14.390	−0.066
0.5	36.46	1.448	0.730	0.083	13.970	−0.051
0.6	36.55	1.514	0.817	0.057	14.070	−0.040
0.8	36.65	1.554	0.876	0.040	13.950	−0.032
1	36.67	1.596	0.946	0.020	13.810	−0.022
1.5	34.11	1.609	1.014	0.003	13.340	−0.014
2	29.34	1.568	1.069	−0.007	12.750	−0.015
3	25.01	1.544	1.048	0.005	13.010	−0.032
4	23.81	1.509	1.003	0.023	13.320	−0.050
5	23.27	1.519	0.947	0.044	13.590	−0.067
6	22.93	1.503	0.916	0.057	13.730	−0.079
8	22.57	1.465	0.916	0.063	13.980	−0.082
10	22.41	1.454	0.943	0.061	14.100	−0.079
15	22.34	1.465	1.051	0.046	14.110	−0.068

glasses were plotted as a function of photon energy at certain penetration depths of 5 mfp and 40 mfp. From this figure, one can see that the BaO content plays an important role in decreasing the EBF values leading to improve the shielding capacity of the glasses. Such that SBC-B35 glass has the lowest values of EBF either at 5 mfp or 40 mfp. Thus, SBC-B35 glass is a promising shielding glass for gamma-ray applications. Fig. 10 demonstrates the behavior of EBF as a function of the penetration depth at specific photon energies such as 0.15, 1, 8, and 10 MeV for all the studied glasses. At 0.15 MeV, The EBF values of all the glasses, except SBC-B00, are independent

of the chemical composition of the glass. Such that SBC-B00 has very large values, while all the other glasses have values around 1. This is attributed to the photoelectric processes which proportional to Z^4 at the low photon energy (i.e. 0.15 MeV). At 1 MeV, EBF values of the studied glasses decrease with increasing the BaO content due to Compton scattering process which proportional to Z at this energy region. At 8 and 10 MeV, the variation of EBF with the penetration depth is completely changed from that at the previous energies. For example, the SBC-B35 glass possesses the highest EBF values, while the SBC-B00 glass possesses the lowest EBF values. This change of the EBF might be interpreted by the pair production processes.

5. Conclusion

SBC-Bx glass system in the chemical composition of $40SiO_2-10B_2O_3-xBaO-(45-x)CaO-yZnO-zMgO$ (where x = 0, 10, 20, 30, and 35 mol% and y = z = 6 mol%) has been successfully investigated in terms of gamma-ray shielding properties. The radiation shielding parameters of the glasses were obtained by using PHITS code and WinXCOM program. The values of μ/ρ generated by using PHITS code agree well with those calculated by using WinXCOM program. The results indicated that the values of μ/ρ, Z_{eff} and N_{eff} increase and the values of HVL, MFP, and EBF decrease with increasing BaO content in the glass sample. For radiation shielding, the selection of an appropriate glass can be done based on data of Z_{eff}, HVL and MFP, consideration of exposure buildup factors and also, according to the desired application. Hence, the SBC-B35 glass is an excellent candidate for shielding applications from gamma-rays among various conventional concrete and commercial glasses. This work on shielding properties of the SBC-Bx glass system would be useful for the scientific community to design, develop or select a proper shielding glass for gamma-ray applications.

Declaration of competing interest

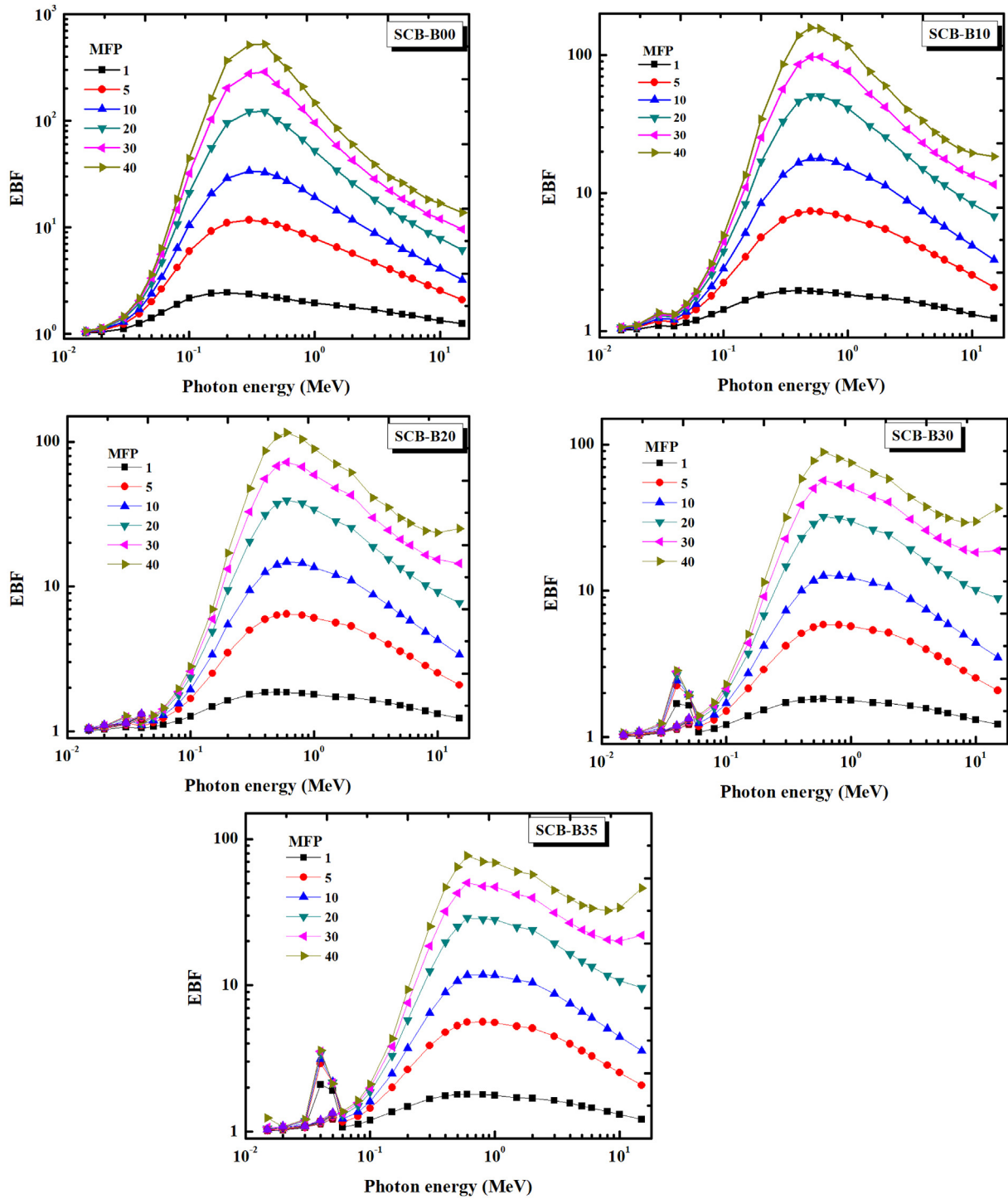We have no conflict of interest to declare.

Fig. 8. The variation of exposure buildup factor (EBF) for each glass with photon energy at different penetration depths 1, 5, 10, 20, 30 and 40 mfp.
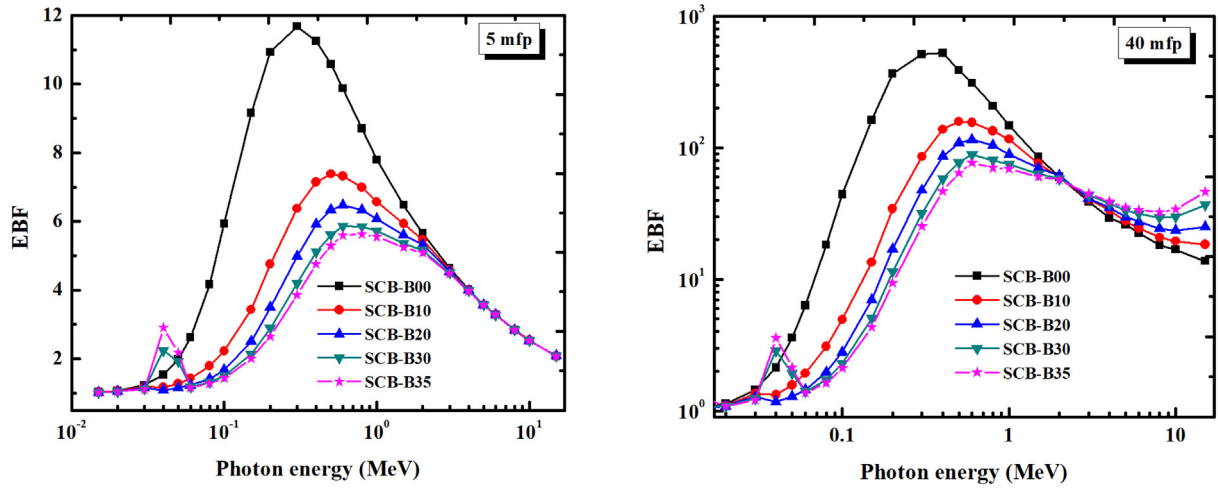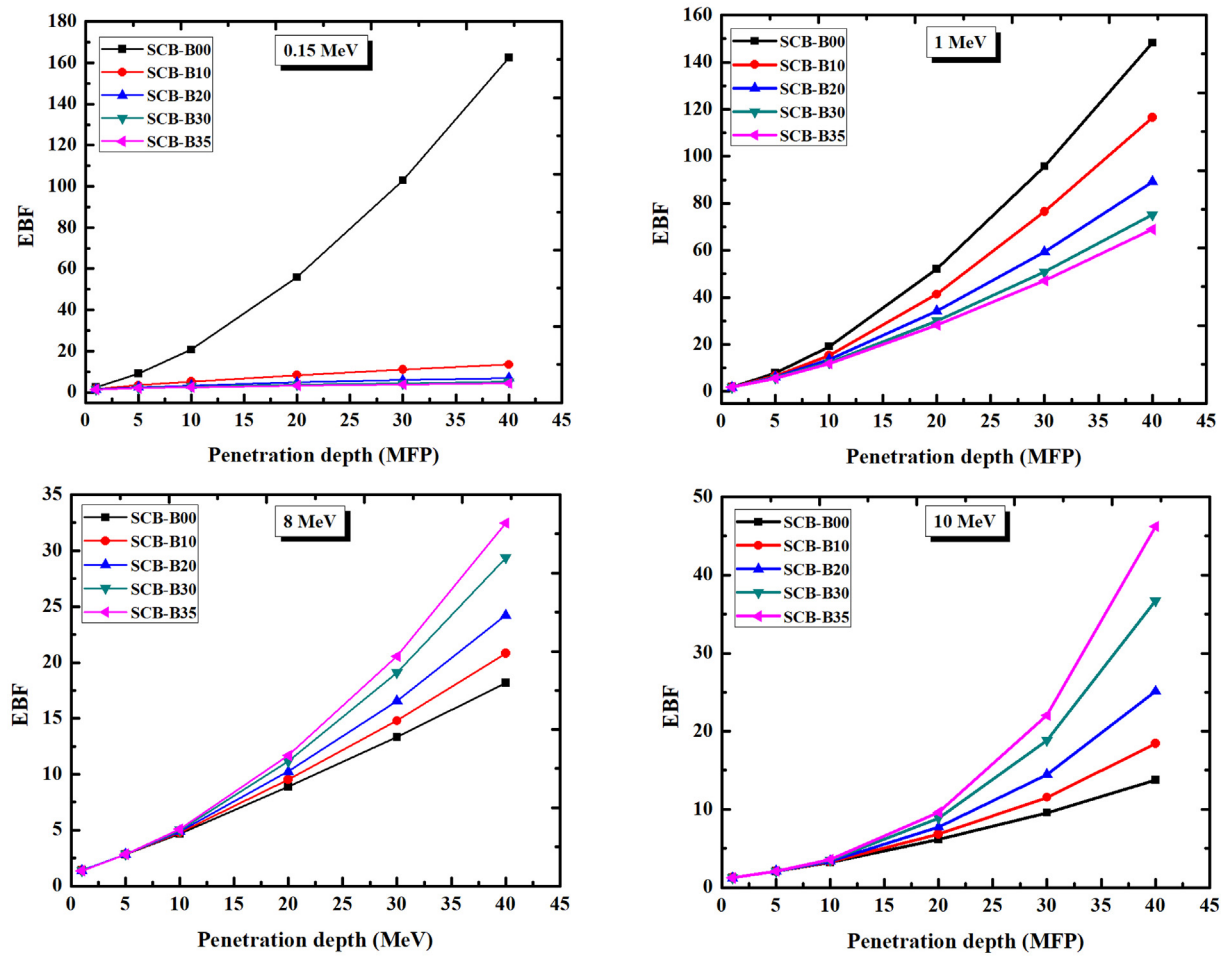
Fig. 9. The variation of exposure buildup factor (EBF) with photon energy for SiO$_2$–B$_2$O$_3$–BaO–CaO–ZnO–MgO glass system at different penetration depths 5 and 40 mfp.

Fig. 10. The variation of exposure buildup factor (EBF) for each glass with photon energy at different penetration depths 1, 5, 10, 20, 30 and 40 mfp.

References

[1] R. Baskar, K.A. Lee, R. Yeo, K.-W. Yeoh, Cancer and radiation therapy: current advances and future directions, Int. J. Med. Sci. 9 (2012) 193.

[2] E. Kavaz, N. Ekinci, H. Tekin, M. Sayyed, B. Aygün, U. Perişanoğlu, Estimation of gamma radiation shielding qualification of newly developed glasses by using winxcom and mcnpx code, Prog. Nucl. Energy 115 (2019) 12–20.

[3] M.S. Al-Buriahi, B.T. Tonguc, Study on gamma-ray buildup factors of bismuth borate glasses, Appl. Phys. A 125 (2019) 482.

[4] M. Al-Buriahi, Y. Alajerami, A. Abouhaswa, A. Alalawi, T. Nutaro, B. Tonguc, Effect of chromium oxide on the physical, optical, and radiation shielding properties of lead sodium borate glasses, J. Non-Cryst. Solids 544 (2020), 120171.

[5] W. Guo-hui, H. Man-li, C. Fan-chao, F. Jun-dong, D. Yao-dong, Enhancement of flame retardancy and radiation shielding properties of ethylene vinyl acetate based radiation shielding composites by eb irradiation, Prog. Nucl. Energy 112 (2019) 225–232.

[6] M. Al-Buriahi, V. Singh, Comparison of shielding properties of various marble concretes using geant4 simulation and experimental data, Journal of the Australian Ceramic Society (2020) 1–7.

[7] M.K.A. Roslan, M. Ismail, A.B.H. Kueh, M.R.M. Zin, High-density concrete: exploring ferro boron effects in neutron and gamma radiation shielding, Construct. Build. Mater. 215 (2019) 718–725.

[8] S.S. Obaid, M. Sayyed, D. Gaikwad, H. Tekin, Y. Elmahroug, P. Pawar, Photon attenuation coefficients of different rock samples using mcnpx, geant4 simulation codes and experimental results: a comparison study, Radiat. Eff. Defect Solid 173 (2018) 900–914.

[9] E.-S.A. Waly, M.A. Bourham, Comparative study of different concrete composition as gamma-ray shielding materials, Ann. Nucl. Energy 85 (2015) 306–310.

[10] S.S. Obaid, M. Sayyed, D. Gaikwad, P.P. Pawar, Attenuation coefficients and exposure buildup factor of some rocks for gamma ray shielding applications, Radiat. Phys. Chem. 148 (2018a) 86–94.

[11] S.S. Obaid, D.K. Gaikwad, P.P. Pawar, Determination of gamma ray shielding parameters of rocks and concrete, Radiat. Phys. Chem. 144 (2018b) 356–360.

[12] D. Yılmaz, B. Aktaş, A. Çalık, O. Aytar, Boronizing effect on the radiation shielding properties of hardox 450 and hardox hituf steels, Radiat. Phys. Chem. 161 (2019) 55–59.

[13] T. Shams, M. Eftekhar, A. Shirani, Investigation of gamma radiation attenuation in heavy concrete shields containing hematite and barite aggregates in multi-layered and mixed forms, Construct. Build. Mater. 182 (2018) 35–42.

[14] M. Kurudirek, N. Chutithanapanon, R. Laopaiboon, C. Yenchai, C. Bootjomchai, Effect of bi2o3 on gamma ray shielding and structural properties of borosilicate glasses recycled from high pressure sodium lamp glass, J. Alloys Compd. 745 (2018) 355–364.

[15] A. Kumar, D. Gaikwad, S.S. Obaid, H. Tekin, O. Agar, M. Sayyed, Experimental studies and Monte Carlo simulations on gamma ray shielding competence of (30+ x) pbo10wo3 10na2o- 10mgo–(40-x) b2o3 glasses, Prog. Nucl. Energy 119 (2020), 103047.

[16] D. Gaikwad, M. Sayyed, S. Botewad, S.S. Obaid, Z. Khattari, U. Gawai, F. Afaneh, M. Shirshat, P. Pawar, Physical, structural, optical investigation and shielding featuresof tungsten bismuth tellurite based glasses, J. Non-Cryst. Solids 503 (2019) 158–168.

[17] S. Souto, M. Massot, M. Balkanski, D. Royer, Density and ultrasonic velocities in fast ionic conducting borate glasses, Mater. Sci. Eng., B 64 (1999) 33–38.

[18] M. Al-Buriahi, A. Abouhaswa, H. Tekin, C. Sriwunkum, F. El-Agawany, T. Nutaro, E. Kavaz, Y. Rammah, Structure, optical, gamma-ray and neutron shielding properties of nio doped b2o3−baco3−li2o3 glass systems, Ceram. Int. 46 (2020) 1711–1721.

[19] M. Al-Buriahi, Y. Rammah, Investigation of the physical properties and gamma-ray shielding capability of borate glasses containing pbo, al 2 o 3 and na 2 o, Appl. Phys. A 125 (2019) 717.

[20] M. Al-Buriahi, K. Mann, Radiation shielding investigations for selected tellurite-based glasses belonging to the tnw system, Mater. Res. Express 6 (2019) 105206.

[21] M. Sayyed, H. Tekin, O. Agar, Gamma photon and neutron attenuation properties of mgo–bao–b2o3–teo2–cr2o3 glasses: the role of teo2, Radiat. Phys. Chem. 163 (2019) 58–66.

[22] E. Kavaz, H. Tekin, N.Y. Yorgun, Ö. Özdemir, M. Sayyed, Structural and nuclear radiation shielding properties of bauxite ore doped lithium borate glasses: experimental and Monte Carlo study, Radiat. Phys. Chem. 162 (2019) 187–193.

[23] M. Sayyed, K.M. Kaky, M. Mhareb, A.H. Abdalsalam, N. Almousa, G. Shkoukani, M.A. Bourham, Borate multicomponent of bismuth rich glasses for gamma radiation shielding application, Radiat. Phys. Chem. 161 (2019) 77–82.

[24] P. Vani, G. Vinitha, M. Sayyed, B. Elbashir, N. Manikandan, Investigation on structural, optical, thermal and gamma photon shielding properties of zinc and barium doped fluorotellurite glasses, J. Non-Cryst. Solids 511 (2019) 194–200.

[25] H. Tekin, E. Kavaz, A. Papachristodoulou, M. Kamislioglu, O. Agar, E.A. Guclu, O. Kilicoglu, M. Sayyed, Characterization of sio2−pbo−cdo−ga2o3 glasses for comprehensive nuclear shielding performance: alpha, proton, gamma, neutron radiation, Ceram. Int. 45 (2019) 19206–19222.

[26] O. Agar, M. Sayyed, H. Tekin, K.M. Kaky, S. Baki, I. Kityk, An investigation on

[27] shielding properties of bao, moo3 and p2o5 based glasses using mcnpx code, Results in Physics 12 (2019) 629–634.

[27] M. Sayyed, A. Kumar, H. Tekin, R. Kaur, M. Singh, O. Agar, M.U. Khandaker, Evaluation of gamma-ray and neutron shielding features of heavy metals doped bi2o3-bao-na2o-mgo-b2o3 glass systems, Prog. Nucl. Energy 118 (2020), 103118.

[28] V.P. Singh, M. Medhat, S. Shirmardi, Comparative studies on shielding properties of some steel alloys using geant4, mcnp, winxcom and experimental results, Radiat. Phys. Chem. 106 (2015a) 255–260.

[29] V. Singh, S. Shirmardi, M. Medhat, N. Badiger, Determination of mass attenuation coefficient for some polymers using Monte Carlo simulation, Vacuum 119 (2015b) 284–288.

[30] A. Askin, M. Sayyed, A. Sharma, M. Dal, R. El-Mallawany, M. Kacal, Investigation ofthe gamma ray shielding parameters of (100-x)[0.5 li2o−0.1 b2o3−0.4 p2o5]-xteo2 glasses using geant4 and fluka codes, J. Non-Cryst. Solids 521 (2019), 119489.

[31] S.A. Issa, Y.B. Saddeek, M. Sayyed, H. Tekin, O. Kilicoglu, Radiation shielding features using mcnpx code and mechanical properties of the pbona2ob2o3-caoal2o3sio2 glass systems, Compos. B Eng. 167 (2019) 231–240.

[32] I. Mahmoud, S.A. Issa, Y.B. Saddeek, H. Tekin, O. Kilicoglu, T. Alharbi, M. Sayyed, T. Erguzel, R. Elsaman, Gamma, neutron shielding and mechanical parameters for lead vanadate glasses, Ceram. Int. 45 (2019) 14058–14072.

[33] Y. Rammah, M. Al-Buriahi, A. Abouhaswa, B2o3−baco3−li2o3 glass system doped with co3o4: structure, optical, and radiation shielding properties, Phys. B Condens. Matter 576 (2020), 411717.

[34] M.S. Al-Buriahi, B.T. Tonguc, Mass attenuation coefficients, effective atomic numbers and electron densities of some contrast agents for computed tomography, Radiat. Phys. Chem. 166 (2020), 108507.

[35] E.-S.A. Waly, M.A. Fusco, M.A. Bourham, Gamma-ray mass attenuation coefficient and half value layer factor of some oxide glass shielding materials, Ann. Nucl. Energy 96 (2016) 26–30.

[36] A. Shimizu, Calculation of Gamma-Ray Buildup Factors up to Depths of 100 Mfp by the Method of Invariant Embedding. (i) Analysis of accuracy and comparison with other data, J. Nucl. Sci. Technol. 39 (2002) 477–486.

[37] G. Lakshminarayana, I. Kebaili, M. Dong, M. Al-Buriahi, A. Dahshan, I. Kityk, D.-E. Lee, J. Yoon, T. Park, Estimation of gamma-rays, and fast and the thermal neutrons attenuation characteristics for bismuth tellurite and bismuth borotellurite glass systems, J. Mater. Sci. 55 (2020) 5750–5771.

[38] M.S. Al-Buriahi, V. Singh, H. Arslan, V. Awasarmol, B.T. Tonguc, Gamma-ray attenuation properties of some nlo materials: potential use in dosimetry, Radiat. Environ. Biophys. 59 (2020a) 145–150.

[39] M. Al-Buriahi, C. Sriwunkum, H. Arslan, B.T. Tonguc, M.A. Bourham, Investigation of barium borate glasses for radiation shielding applications, Appl. Phys. A 126 (2020b) 1–9.

[40] I. Han, L. Demir, Studies on effective atomic numbers, electron densities from mass attenuation coefficients in tixco1- x and coxcu1- x alloys, Nucl. Instrum. Methods Phys. Res. Sect. B Beam Interact. Mater. Atoms 267 (2009) 3505–3510.

[41] M. Kurudirek, Effective atomic numbers and electron densities of some human tissues and dosimetric materials for mean energies of various radiation sources relevant to radiotherapy and medical applications, Radiat. Phys. Chem. 102 (2014) 139–146.

[42] M. Al-Buriahi, H. Arslan, H. Tekin, V. Singh, B.T. Tonguc, Moo3-teo2 glass system for gamma ray shielding applications, Mater. Res. Express 7 (2020), 025202.

[43] S. Manohara, S. Hanagodimath, L. Gerward, S. Subhranshu, Energy-absorption buildup factors of some fluorides and sulfates: thermoluminescent dosimetric materials, Mater. Today: Proceedings 10 (2019) 20–24.

[44] P. Kaur, K. Singh, M. Kurudirek, S. Thakur, Study of environment friendly bismuth incorporated lithium borate glass system for structural, gamma-ray and fast neutron shielding properties, Spectrochim. Acta Mol. Biomol. Spectrosc. 223 (2019), https://doi.org/10.1016/j.saa.2019.117309, 117309.

[45] M.S. Al-Buriahi, H. Arslan, B.T. Tonguc, Investigation of photon energy absorption properties for some biomolecules, Nucl. Sci. Tech. 30 (2019) 103.

[46] M. Kurudirek, Heavy metal borate glasses: potential use for radiation shielding, J. Alloys Compd. 727 (2017) 1227–1236.

[47] A. Abouhaswa, M. Mhareb, A. Alalawi, M. Al-Buriahi, Physical, structural, optical, and radiation shielding properties of b2o3-20bi2o3-20na2o2-sb2o3 glasses: role of sb2o3, J. Non-Cryst. Solids 543 (2020), 120130.

[48] ANSI/ANS-6.4.3, Gamma Ray Attenuation Coefficient and Buildup Factors for Engineering Materials, 1991.

[49] T. Sato, Y. Iwamoto, S. Hashimoto, T. Ogawa, T. Furuta, S.-i. Abe, T. Kai, P.-E. Tsai, N. Matsuda, H. Iwase, et al., Features of particle and heavy ion transport code system (phits) version 3.02, J. Nucl. Sci. Technol. 55 (2018) 684–690.

[50] A. Kumar, Gamma ray shielding properties of pbo-li2o-b2o3 glasses, Radiat. Phys. Chem. 136 (2017) 50–53.

[51] M.S. Al-Buriahi, B.T. Tonguc, Mass attenuation coefficients, effective atomic numbers and electron densities of some contrast agents for computed tomography, Radiat. Phys. Chem. 166 (2020), 108507.

[52] M.S. Al-ahi, H. Arslan, B.T. Tonguç, et al., Mass attenuation coefficients, water and tissue equivalence properties of some tissues by geant4, xcom and experimental data, Indian J. Pure Appl. Phys. 57 (2019) 433–437.

[53] H.-X. Shi, B.-X. Chen, T.-Z. Li, D. Yun, Precise Monte Carlo simulation of gamma-ray response functions for an nai (tl) detector, Appl. Radiat. Isot. 57 (2002) 517–524.

[54] M.J. Berger, J. Hubbell, XCOM: Photon Cross Sections on a Personal Computer, Technical Report, National Bureau of Standards, Center for Radiation Research, Washington, DC (USA), 1987.

[55] M.S. Al-Buriahi, H. Arslan, B.T. Tonguc, Investigation of photon energy absorption properties for some biomolecules, Nucl. Sci. Tech. 30 (2019) 103.

[56] P. Kaur, K. Singh, S. Thakur, P. Singh, B. Bajwa, Investigation of bismuth borate glass system modified with barium for structural and gamma-ray shielding properties, Spectrochim. Acta Mol. Biomol. Spectrosc. 206 (2019) 367–377.

[57] P. Fuochi, U. Corda, M. Lavalle, A. Kovács, M. Baranyai, A. Mejri, K. Farah, Dosimetric properties of gammaand electron-irradiated commercial window glasses, Nukleonika 54 (2009) 39–43.

[58] I. Bashter, Calculation of radiation attenuation coefficients for shielding concretes, Ann. Nucl. Energy 24 (1997) 1389–1401.

[59] Y. Elmahroug, M. Almatari, M. Sayyed, M. Dong, H. Tekin, Investigation of radiation shielding properties for bi2o3-v2o5-teo2 glass system using mcnp5 code, J. Non-Cryst. Solids 499 (2018) 32–40.